JPL D-100521

Multiangle SpectroPolarimetric Imager

Cloud Droplet Size and Cloud Optical Depth Retrieval Algorithm Theoretical Basis

Feng Xu[1]
David J. Diner[1]
James L. McDuffie[1]
Michael J. Garay[1]
Irina N. Tkatcheva[1]
Michael A. Bull[1]
Felix C. Seidel[1]
Gerard van Harten[1]
Anthony B. Davis[1]
Larry Di Girolamo[2]
Dongwei Fu[2]
Ming Su[2]
Guangyu Zhao[2]

[1]Jet Propulsion Laboratory, California Institute of Technology
[2]Department of Atmospheric Sciences, University of Illinois

Jet Propulsion Laboratory
California Institute of Technology

January 17, 2018

JPL D-100521

Airborne Multiangle SpectroPolarimetric Imager (AirMSPI)

Cloud Droplet Size and Cloud Optical Depth Retrieval Algorithm Theoretical Basis

Approval:

David J. Diner
AirMSPI Principal Investigator

Earl G. Hansen
AirMSPI Project Manager

The AirMSPI web site should be consulted to determine the latest released version of this document (https://eosweb.larc.nasa.gov/project/airmspi/)
Approval signatures are on file with the AirMSPI Project.

Jet Propulsion Laboratory
California Institute of Technology

TABLE OF CONTENTS

LIST OF TABLES

LIST OF FIGURES

GLOSSARY OF ACRONYMS

A

ADS (AirMSPI Droplet Size)
AirMSPI (Airborne Multiangle SpectroPolarimetric Imager)
ADSD (AirMSPI Droplet Size Dataset)
ASDC (Atmospheric Sciences Data Center)
ATB (Algorithm Theoretical Basis)

D

DoLP (Degree of Linear Polarization)

J

JPL (Jet Propulsion Laboratory)

L

LaRC (Langley Research Center)
Look-up-table (LUT)

M

MISR (Multi-angle Imaging SpectroRadiometer)

R

RDQI (Radiometric Data Quality Indicator)

S

SAMS (Simulated Ancillary Mie Scattering)

SART (Simulated Ancillary Radiative Transfer)

W

WGS84 (World Geodetic System of 1984)

1 INTRODUCTION

1.1 PURPOSE

The AirMSPI Cloud Droplet Size and Cloud Optical Depth Retrieval Algorithm Theoretical Basis (ATB) documents the algorithm for determining cloud-top droplet size distribution and 1D radiative transfer (RT) based cloud optical depth from AirMSPI polarimetric measurements in the vicinity of the cloudbow. The parameters output from the retrieval are summarized in Table 1.

In particular, this document identifies the sources of input data required for the retrieval, provides the physical theory and mathematical background underlying the use of AirMSPI data in the retrievals, and describes key assumptions and limitations of the adopted approach. This document is used by the AirMSPI Science Data System Team to establish requirements and functionality of the data processing software.

Table 1: Cloud Droplet Size and Cloud Optical Depth Retrieval Product Output

Parameter name	Units	Description
Name of L1B2 input file	-	Cloud image file name
Acquisition start time	-	Specified as "YYYY-MM-DD, HH:MM:SS UTC", e.g., "2013-08-15, 00:00:00 UTC"
Acquisition end time	-	Specified as "YYYY-MM-DD, HH:MM:SS UTC", e.g., "2013-08-15, 00:00:00 UTC"
Upper left latitude	degrees	Geographic latitude of cloud image in the upper left corner of the granule (Degrees N)
Upper left longitude	degrees	Geographic longitude of center of cloud image in the upper left corner of the granule (Degrees E)
Upper right latitude	degrees	Geographic latitude of cloud image in the upper right corner of the granule (Degrees N)
Upper right longitude	degrees	Geographic longitude of center of cloud image in the upper right corner of the granule (Degrees E)
Lower left latitude	degrees	Geographic latitude of cloud image in the Lower left corner of the granule (Degrees N)
Lower left longitude	degrees	Geographic longitude of center of cloud image in the Lower left corner of the granule (Degrees E)
Lower right latitude	degrees	Geographic latitude of cloud image in the Lower right corner of the granule (Degrees N)
Lower right longitude	degrees	Geographic longitude of center of cloud image in the Lower right corner of the granule (Degrees E)
Effective radius	μm	For Gamma distribution of droplet size
Effective variance	-	For Gamma distribution of droplet size
Effective radius uncertainty	μm	Uncertainty of the retrieved effective radius
Effective variance uncertainty	-	Uncertainty of the retrieved effective variance
Other empirical fitting parameters and uncertainties	-	For empirically correct fraction of cloud coverage, above-cloud aerosol contamination and other unmodeled effects
Observed polarized phase function	-	Corrected from the measured Stokes component Q
Modeled polarized phase function	-	Evaluated using the optimized solution

Reduced Chi-square residue of polarized phase function	-	Evaluated using observed and modeled polarized phase function
Cloud optical depth	-	Evaluated at three polarimetric bands
Cloud optical depth uncertainty	-	Evaluated at three polarimetric bands
Observed pixel radiance	Sr^{-1}	Normalized by Earth-Sun distance and solar irradiance
Modeled pixel radiance	Sr^{-1}	At three polarimetric bands
Reduced Chi-square residue of pixel radiance	-	-
Longitude of pixels used for cloud optical depth retrieval	degrees	-
Latitude of pixels used for cloud optical depth retrieval	degrees	-
Retrieval quality indicator	-	Integer between 1 and 5 to estimate retrieval quality

1.2 SCOPE

This document covers the ATB for the AirMSPI Cloud-Top Droplet Size and Cloud Optical Depth product. Specialized products or parameters are not discussed. Current development and prototyping efforts may result in modifications to parts of the algorithm.

Chapter 1 describes the purpose and scope of the document. Chapter 2 provides a brief overview. The processing concept and algorithm description are presented in Chapter 3. Chapter 4 summarizes assumptions and limitations.

1.3 AirMSPI DOCUMENTS

Reference to AirMSPI reference documents is indicated by a number in square brackets as follows, e.g., [A-1]. The AirMSPI website at ASDC (https://eosweb.larc.nasa.gov/project/airmspi/) should be consulted to determine the latest released version of each of these documents.

[A-1]. Data Product Specification for the AirMSPI Level 1B2 Products, JPL D-100523.

[A-2]. User Guide for the AirMSPI Level 1B2 Products, JPL D-78962.

1.4 REVISIONS

This is the first issue of this document. Future versions will be marked with a revision designation.

2 EXPERIMENT OVERVIEW

2.1 OBJECTIVES OF AirMSPI CLOUD-TOP DROPLET SIZE AND CLOUD OPTICAL DEPTH PRODUCT

The overall objectives of AirMSPI warm cloud water droplet size and cloud optical depth retrievals are to study:

(1) droplet size distribution within liquid water clouds;

(2) how these cloud properties depend on the local environment.

2.2 INSTRUMENT CHARACTERISTICS

AirMSPI is an ultraviolet/visible/near-infrared (UV/VNIR) pushbroom camera. Mounted on a gimbal, it makes multi-angular observations over a ±67° along-track range. The nominal band center wavelengths and bandpass specifications (shown in parentheses) provided to the filter manufacturer were 355(30), 380(32), 445(36), 470(37), 555(31), 660(42), 865(39), and 935(48) nm. Using a dual photoelastic retardance modulator system [Diner et al., 2007] and synchronous demodulation, images of radiance (I) and Stokes vector components Q and U are obtained in the 470, 660 and 865 nm bands. At other bands, only images of radiance (I) are acquired.

AirMSPI has been flying aboard the NASA ER-2 research aircraft at a nominal altitude of 20 km since 2010. It has two operation modes: "step-and-stare" and "continuous sweep." In "step and stare" mode, the camera is pointed at the same target area at a fixed set of view angles beginning with the most forward view and then stepping aftward as the aircraft flies downtrack. The camera then slews forward and the sequence repeats for the next target, about 100 km down track. This mode is most useful where the highest possible spatial resolution (~10 m) is desired. Target area is ~10.6 km cross-track (at nadir) × 9.5 km along-track for a nominal sequence containing nine view angles. An odd number of "stares" is typically selected so that the images are acquired for a set of symmetric view angles forward and aftward of the nadir (0°) view angle. The along-track sample spacing (8 m at any angle) is set by the frame time and aircraft speed. In "continuous sweep" mode, the gimbal slews back and forth. Because the gimbal moves continuously, spatial resolution is reduced to ~ 25 m to account for this effect. However, this mode enables better spatial and angular coverage of cloud fields over a scale of several hundreds of kilometers.

In both "step-and-stare" and "continuous sweep" modes, AirMSPI frequently observes the polarized cloudbow. The appearance of cloudbow, glory and supernumeraries and symmetry around the backward scattering direction in "continuous sweep" observation mode indicate spherical cloud droplets. The angular positions and relative magnitudes of cloudbow fringes are determined by the droplet size distribution at the cloud top.

Additional background on the AirMSPI instrument design is provided in Diner et al. (2007, 2013).

2.3 RETRIEVAL STRATEGY

In order to constrain the droplet size retrieval, we adopt the conventional cloud physics

assumption that droplet size distribution conforms to the Gamma distribution, which is characterized by two parameters: effective radius and effective variance. The range of effective radius and effective variance used in the retrieval are listed in Sections 6.2 and 6.3. Moreover, the refractive indices of water droplets are taken from pure water droplets at the temperature 19ºC (Daimon and Masumura, 2007). The values are given in Table 3 of Section 6.1. The cloud optical depth retrieval is based on 1D RT theory. The grids of cloud optical depth in the lookup table are given in Section 6.5.

A summary of the AirMSPI cloud droplet size and cloud optical depth retrieval strategy is as follows: Based on the refractive index and gridded effective radius and variance of droplet size distribution, Mie scattering calculations in full scattering angular range were performed to provide the polarized phase function P_{12} at the three AirMSPI polarimetric bands, using code developed at the JPL. The Simulated Ancillary Mie Scattering Dataset for polarized phase function was then generated for all combinations of effective radius and effective variance. The pre-calculated results are used in conjunction with the AirMSPI observations of Stokes component Q to determine the best size distribution that fits the observation with minimum fitting error. After the cloud droplet size is determined, the cloud optical depth is retrieved by fitting the lookup table radiance for the retrieved droplet size distribution. The lookup table radiances are calculated using JPL Markov chain radiative transfer code for various combination of cloud droplet effective radius, effective variance, cloud optical depth, solar zenith angle, viewing angle and relative azimuth angles at their gridded values, and save in the six-dimensional Simulated Ancillary Radiative Transfer Dataset. Interpolation is used to determine the pixel-resolved local lookup table of radiances at the specific retrieved droplet size distribution and viewing/incidence geometries.

3 ALGORITHM DESCRIPTION

3.1 PROCESSING OUTLINE

Processing flow concepts are shown diagrammatically throughout the document. The convention for the various elements displayed in these diagrams is shown in Figure 1.

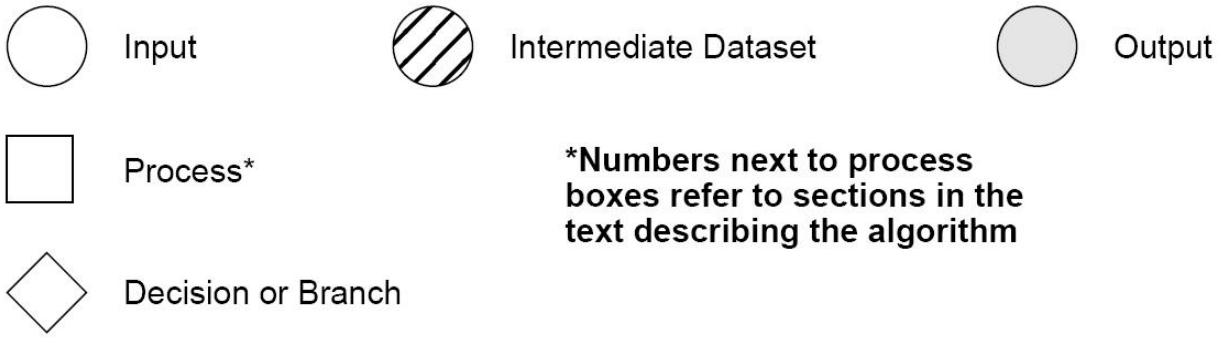

Figure 1. Conventions used in processing flow diagrams

The cloud droplet size and cloud optical depth retrieval process is assisted by establishing two ancillary datasets. These are:

(1) The AirMSPI Droplet Size (ADS) Dataset, which consists of a droplet microphysical property file containing a) droplet refractive indices for the three AirMSPI polarimetric bands; b) droplet size distribution table containing grids of effective radius and effective variance; c) scattering angular grids at which polarized phase function is calculated and solar incidence/viewing/relative azimuthal angular grids and optical depth grids at which radiance is calculated; d) Gaussian quadrature points of droplet radius for Mie scattering computation; and e) optical properties file containing scattering characteristics of all size distribution candidates in the look-up table (LUT), including extinction and scattering cross-sections.

(2) The three-dimensional Simulated Ancillary Mie Scattering (SAMS) Dataset, which contains the polarized phase functions computed by Mie theory as a function of scattering angle, effective radius and effective variance used in the ADS Dataset.

(3) The six-dimensional Simulated Ancillary Radiative Transfer (SART) Dataset, which contains the radiance computed by Markov chain radiative transfer model [Xu et al. 2016] as a function of solar incidence angle, viewing angle, relative azimuthal angle, effective radius, effective variance, and cloud optical depth used in the ADS Dataset.

In addition to the two above datasets, a Retrieval Configuration File (RCF) is also used to assist the retrieval. In such a file, all retrieval configuration parameters, including minimum and

maximum scattering angles, scattering angle resolution, Critical Radiometric Data Quality Indicator, maximum iteration step, convergence criterion for effective radius and variance, and criterion for reduced Chi-square fitting error are specified. As to be described later, the default values of these parameters are based on our algorithm test or references.

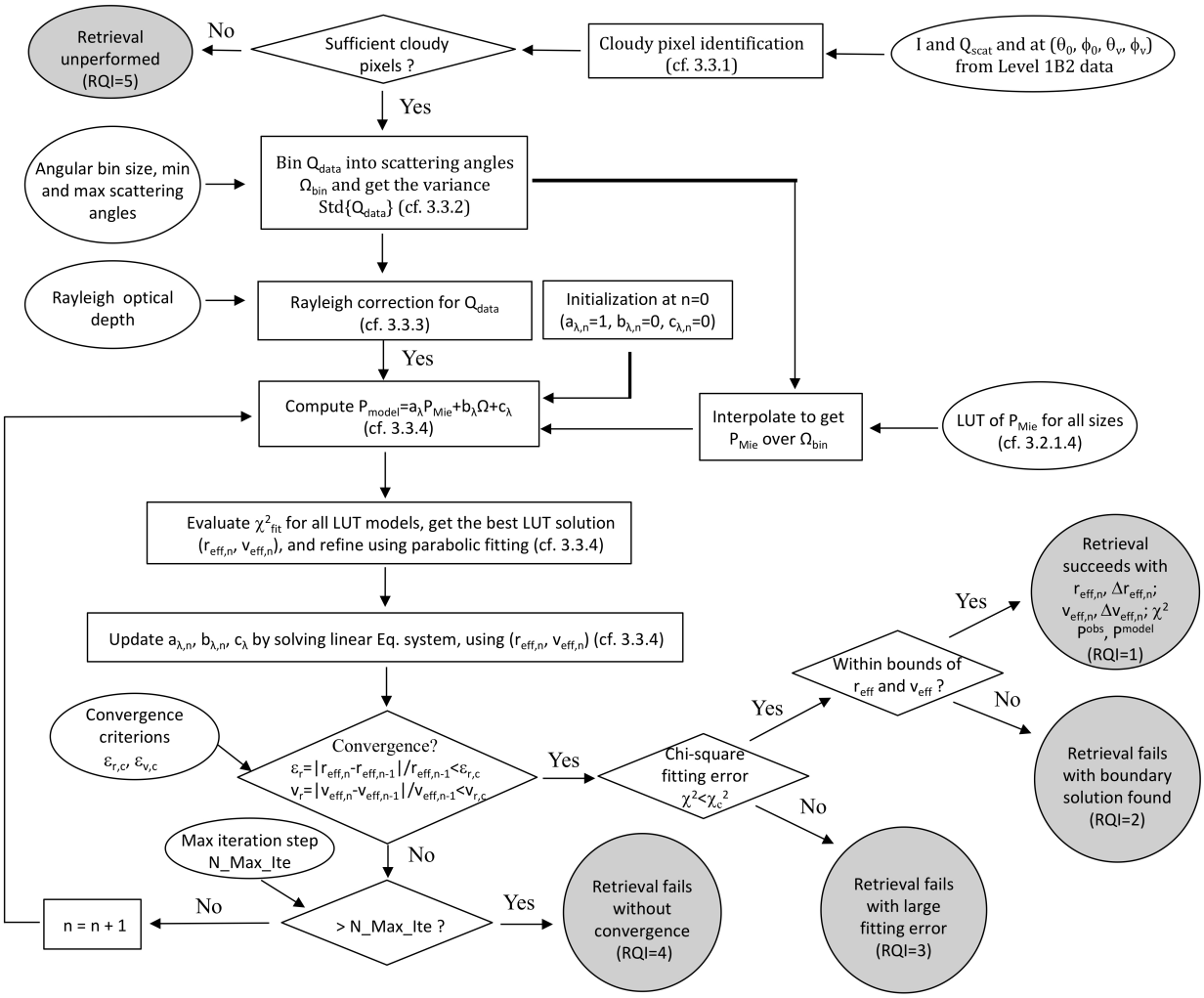

Figure 2. Cloud-top droplet size retrieval algorithm overview (cf. Section 3.3 for symbols)

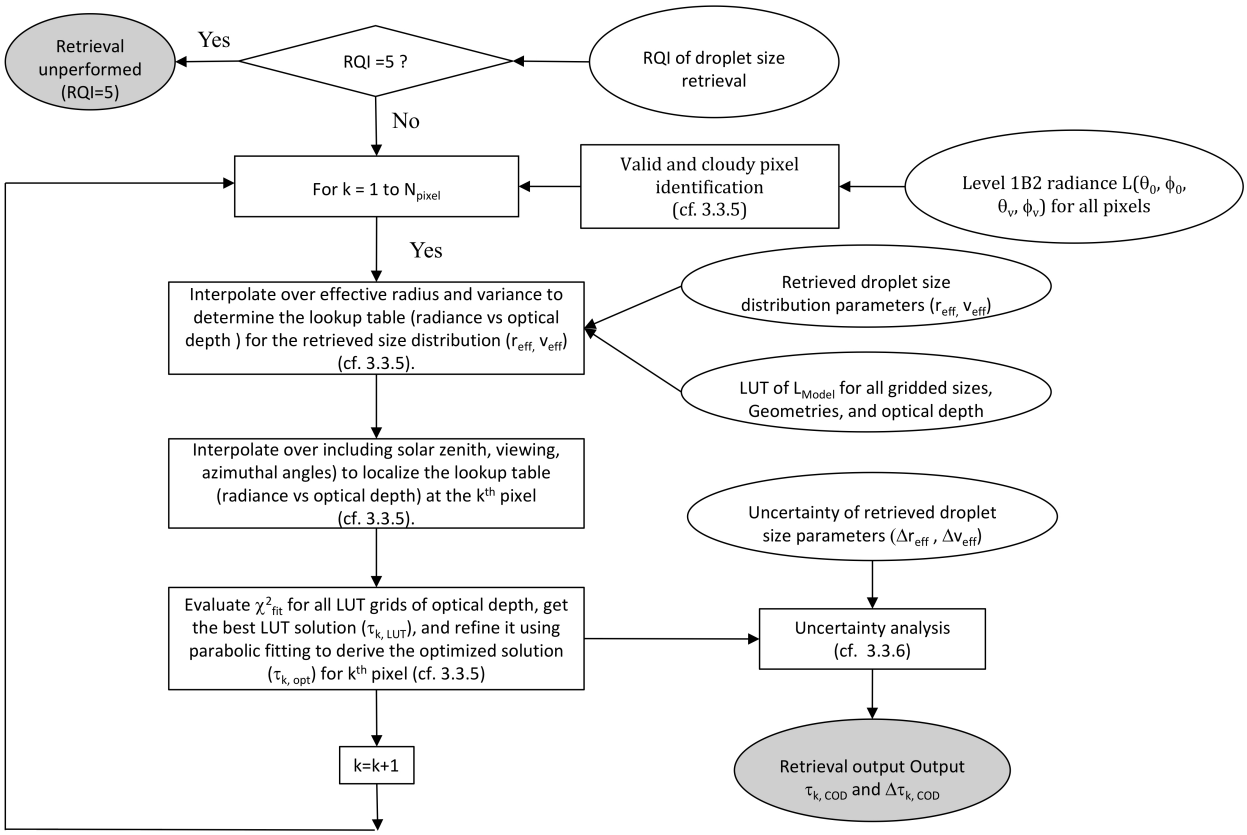

Figure 3. Cloud optical depth retrieval algorithm overview (cf. Section 3.3 for symbols)

3.2 ALGORITHM INPUT

3.2.1 AirMSPI data

The required inputs for the droplet size retrieval are summarized in Table 2 (also cf. the algorithm flow charts Figs. 2 and 3 for droplet size and cloud optical depth retrieval, respectively).

Table 2: Cloud Droplet Size and Cloud Optical Depth Retrieval Product Input

Input data	Source of data	Default value	Reference
Stokes vector component Q relative to the scattering plane	Level 1B2 Ellipsoid-Projected Product	-	[A-1]
Valid Q Data Location Indicator (Q.mask)	Level 1B2 Ellipsoid-Projected Product	-	[A-1]
Solar zenith angle relative to overhead sun (0°)	Level 1B2 Ellipsoid-Projected Product	-	[A-1]
Solar azimuth angle relative to North (0°)	Level 1B2 Ellipsoid-Projected Product	-	[A-1]
View zenith angle relative to nadir (0°)	Level 1B2 Ellipsoid-Projected Product	-	[A-1]
View azimuth angle relative to North (0°)	Level 1B2 Ellipsoid-Projected Product	-	[A-1]
Sun distance	Level 1B2 Ellipsoid-Projected Product	-	[A-1]
Solar irradiance	Level 1B2 Ellipsoid-Projected Product	-	[A-1]
Start time of acquisition	Level 1B2 Ellipsoid-Projected Product	-	[A-1]
End time of acquisition	Level 1B2 Ellipsoid-Projected Product	-	[A-1]
Upper left Geographic Latitude	Level 1B2 Ellipsoid-Projected Product	-	[A-1]
Upper left Geographic Longitude	Level 1B2 Ellipsoid-Projected Product	-	[A-1]

Input data	Source of data	Default value	Reference
Upper right Geographic Latitude	Level 1B2 Ellipsoid-Projected Product	-	[A-1]
Upper right Geographic Longitude	Level 1B2 Ellipsoid-Projected Product	-	[A-1]
Lower left Geographic Latitude	Level 1B2 Ellipsoid-Projected Product	-	[A-1]
Lower left Geographic Longitude	Level 1B2 Ellipsoid-Projected Product	-	[A-1]
Lower right Geographic Latitude	Level 1B2 Ellipsoid-Projected Product	-	[A-1]
Lower right Geographic Longitude	Level 1B2 Ellipsoid-Projected Product	-	[A-1]
Effective Radius Grids	ADS Dataset	-	Section 6.2
Effective Variance Grids	ADS Dataset	-	Section 6.3
Polarized Scattering Function	SAMS Dataset	-	-
Model radiance	SART Dataset	-	-
Min Scattering angle in retrieval (Min_Sca_Re)	Retrieval Configuration File	135º	Section 3.3.2
Max Scattering angle in retrieval (Max_Sca_Re)	Retrieval Configuration File	160º	Section 3.3.2
Bin resolution of scattering angle (Del_Sca)	Retrieval Configuration File	0.125º	Section 3.3.2
Rayleigh scale height (HR)*	Retrieval Configuration File	8.0 km	Section 3.3.3
Depolarization factor of Rayleigh scattering (Delta_R)	Retrieval Configuration File	0.029	Section 3.3.3
Cloud-top height (HCT)**	Retrieval Configuration File	1.0 km	Section 3.3.3
Maximum iteration step (N_Max_Ite)	Retrieval Configuration File	15	Section 3.3.4
Convergence criterion for effective radius (Eps_reff)	Retrieval Configuration File	0.03	Section 3.3.4

Input data	Source of data	Default value	Reference
Convergence criterion for effective variance (Eps_veff)	Retrieval Configuration File	0.03	Section 3.3.4
Criterion for reduced Chi-square fitting error (Chi_Cri)	Retrieval Configuration File	100	Section 3.3.4

* assuming 101.3 kPa at sea level. The atmosphere above aircraft altitude is neglected and gas absorption is empirically accounted (cf. Section 3.3.4).
** Constant values assumed for a whole cloud scene.

3.2.1.1 Ellipsoid-projected radiance and Stokes parameters

In this projection, the surface is assumed to correspond to the WGS84 ellipsoid. To access signals, Stokes vector component I and Q at 470, 660, and 865 nm bands must be ingested for cloudy pixel identification and retrieval. The data fields I.mask and Q.mask take the values of 1 and 0 for valid and invalid data, respectively.

3.2.1.2 Ellipsoid-referenced geometric parameters

The ellipsoid-referenced geometric parameters are calculated at Level 1B2, and provide view zenith and azimuth angles as well as solar zenith and azimuth angles. Taking 470 nm as an example, they are obtained from

/HDFEOS/GRIDS/470nm_band/Data Fields/View_zenith,
/HDFEOS/GRIDS/470nm_band/Data Fields/View_azimuth,
/HDFEOS/GRIDS/470nm_band/Data Fields/Sun_zenith,
/HDFEOS/GRIDS/470nm_band/Data Fields/Sun_azimuth, and
/HDFEOS/GRIDS/470nm_band/Data Fields/Scattering_angle,

respectively. Changing the wavelength number from 470 nm to 660 and 865 nm gives the geometric parameters at all other bands.

3.2.1.3 Band-weighted exo-atmospheric solar irradiances

Band-weighted exo-atmospheric solar irradiances are denoted as $E_{0,\lambda}$. They were calculated by averaging the spectral values of Wehrli (1985) over the nominal FWHM bandpass values and can be obtained from /Channel_Information/SolarIrradianceAt1AU.

3.2.1.4 Earth-Sun distance

The Earth-Sun distance is denoted as *d*. It is in Astronomical Unit and obtained from /HDFEOS/ADDITIONAL/FILE_ATTRIBUTES/Sun distance.

3.2.1.5 Other relevant ancillary data

Acquisition start and end time (in UTC) are obtained from
/HDFEOS/ADDITIONAL/FILE_ATTRIBUTES/Acquisition start time
/HDFEOS/ADDITIONAL/FILE_ATTRIBUTES/Acquisition end time

respectively.

The upper left latitude (degrees N) and longitude (degrees E), upper right latitude and longitude, lower left latitude and longitude, and lower right latitude and longitude of cloud image are obtained from

/HDFEOS/ADDITIONAL/FILE_ATTRIBUTES/Upper left latitude
/HDFEOS/ADDITIONAL/FILE_ATTRIBUTES/Upper left longitude
/HDFEOS/ADDITIONAL/FILE_ATTRIBUTES/Upper right latitude
/HDFEOS/ADDITIONAL/FILE_ATTRIBUTES/Upper right longitude
/HDFEOS/ADDITIONAL/FILE_ATTRIBUTES/Lower left latitude
/HDFEOS/ADDITIONAL/FILE_ATTRIBUTES/Lower left longitude
/HDFEOS/ADDITIONAL/FILE_ATTRIBUTES/Lower right latitude
/HDFEOS/ADDITIONAL/FILE_ATTRIBUTES/Lower right longitude

respectively. Together with the acquisition time, these data are reported in the product.

3.2.1.6 Optical properties of droplets and radiance of cloud

In the SAMS dataset, the polarized phase functions are computed for all combinations of effective radius and effective variance at their grids. The results are saved in the HDF5 files under the name "P12Wave1.h5", "P12Wave2.h5", and "P12Wave3.h5" for the 470, 660 and 865 nm bands, respectively. In these files, the field "/scattering" contains the polarized phase functions, which is a two-dimensional matrix of cells: one dimension of the matrix corresponds to effective radius and the other to effective variance. Each cell is associated with a grid containing an array of polarized phase function (P_{12}) as a function of scattering angles. P_{12} is calculated for spherical droplets using a Mie code developed at JPL referring to Shen and Cai (2005). The scattering angles are saved in the ADS with the field name "Header/thetas_grid".

In the SART dataset, the radiances are computed for all combinations of cloud optical depth, solar zenith angle, viewing angle, relative azimuthal angle, effective radius and effective variance at their grids. The results are saved in the HDF5 files under the name "/nwave(i)nr(j)nv(k)ntheta0(m).h5" where i^{th} spectral band, j^{th} effective radius grid, k^{th} effective variance grid, m^{th} grid of solar zenith angle. In these files, the field "/L" contains the radiance matrix, which is a three-dimensional matrix: the first dimension corresponds to viewing angle, the second dimension corresponds to relative azimuthal angle, and the third dimension corresponds to the cloud optical depth. Grid setting for all dimensions is described in Appendix 6.

3.3 THEORETICAL DESCRIPTION:

ADS retrieval consists of seven major steps: identifying cloudy pixels (cf. 3.3.1) from the radiance (I), binning signals of Stokes vector component Q into scattering bins (cf. 3.3.2), performing Rayleigh correction (cf. 3.3.3), retrieval of droplet size distribution from polarized phase function (cf. 3.3.4) and cloud optical depth from pixel radiance (cf. 3.3.5), retrieval uncertainty analysis (cf. 3.3.6), and then product generation (cf. 3.3.7).

3.3.1 Cloudy pixel identification

We designed a cloud mask algorithm by setting a geometry dependent threshold values for

the radiance observed at the 660 nm spectral band: the pixels with $I_{660nm} > I_{cld,\ thres}$ are identified as the cloudy pixels and their Q data are collected for retrieval. For implementation, pixels with valid Q signals from all the three polarimetric bands are prepared for further application of the cloudy pixel identification algorithm using the valid radiance from 660 nm (I.mask=1 for 660 nm). To determine "$I_{cld,\ thres}$", radiative transfer computation by use of a hybrid method combining Markov chain and doubling-adding models [Xu et al. 2016] was performed to calculate the radiance for different combinations of effect radius and effective variance within their ranges of 5 to 20 μm and 0.001 to 0.4 and pick up the smallest value of radiance for each set of viewing and azimuthal angles. Computations were performed for a cloud optical depth 2 and the lookup table of solar zenith angle from 0° to 85° with 5° angular resolution, viewing angle from 0° to 90° with 1° angular resolution and azimuthal angle from 0° to 360° with 2° angular resolution. Linear interpolation is then implemented to get the threshold value "$I_{cld,\ thres}$" for a particular scenario of cloud image with known solar incidence angle and viewing geometry including viewing and azimuthal angles. Specifically, two steps are taken: 1) the average solar zenith angle for all pixels to be used in the scene is calculated; 2) we use this average solar zenith angle to linearly interpolate "$I_{cld,\ thres}$" over solar zenith angle; 3) we use the per-pixel geometry to bilinearly interpolate "$I_{cld,\ thres}$" over viewing zenith angle and relative azimuthal angle.

3.3.2 Discretization of Q signals into scattering angular bins

The purpose of this step is to read Level 1B2 input Stokes vector component data Q and ellipsoid-referenced geometric parameters and bin the Q signals into scattering angles. The step of binning is to reduce the data redundancy and speed up retrieval.

At each pixel sample (i, j), the scattering angle (Ω) available from L1B2 data is computed by

$$\cos\Omega(i,j) = -\mu(i,j)\mu_0(i,j) + \nu(i,j)\nu_0(i,j)\cos[\phi(i,j) - \phi_0(i,j)], \quad (1)$$

where μ and μ_0 are cosines of the viewing and solar zenith angles, respectively, ν and ν_0 are sines of the viewing and solar zenith angles, respectively, and ϕ and ϕ_0 are viewing and solar azimuthal angles, respectively (see 3.2.1.2).

Note that all angles in Eq. (1) have wavelength dependence, which are accounted in the retrieval. For simplicity, however, the wavelength dependence is dropped off in all equations throughout this ATBD.

In some situations, using Q signals in a confined azimuthal range ($2\Delta\phi_c$) around principal plane is favorable. The AirMSPI observations, however, were not always made around the principal plane. Therefore, valid Q-data in all azimuthal planes are taken into account to cover the most general situations of observation.

The Q signals in the scattering angular range $\Omega_{min,\ re} \le \Omega \le \Omega_{max,\ re}$ are used for retrieval. And $\Omega_{min,\ re}$ and $\Omega_{max,\ re}$ are set via "thetas_min_re" and "thetas_max_re" in the RCF, respectively. Referring to Bréon and Goloub (1998) and Alexandrov et al. (2012), and $\Omega_{min,\ re}$ and $\Omega_{max,\ re}$ are set as 135° and 160°, respectively. We don't recommend using the Q-signals beyond $\Omega < 130°$ and $\Omega > 165°$ for droplet size retrieval as the polarized radiance can be contaminated by the

contribution of multiple scattering, aerosol above cloud and cloud top pressure. The angular resolution $\Delta\Omega_{sca}$ for data acquisition is set via "Del_Sca" in RCF. The default value of $\Delta\Omega_{sca}$ is set as 0.125° to resolve cloudbow fringes for a large droplet size with narrow distribution (cf. Section 6.2).

Averaging over all applicable samples of Stokes vector component Q in a given scattering angular bin is required. It is realized in the following way to generate the output $\bar{Q}_{n_b}^{\text{Obs}}$ and the standard deviation $\sigma_{Q_{n_b}^{\text{Obs}}}$ in the n_b^{th} scattering angular bin:

$$\bar{Q}_{n_b}^{\text{Obs}} = \frac{\sum_{i,j} M_Q(i,j) Q(i,j)}{\sum_{i,j} M_Q(i,j)}, \tag{2}$$

$$\sigma_{Q_{n_b}^{\text{Obs}}} = \sqrt{\frac{\sum_{i,j} M_Q(i,j)\left[Q(i,j) - \bar{Q}_{n_{\text{bin}}}^{\text{Obs}}\right]^2}{\sum_{i,j} M_Q(i,j) - 1}}, \tag{3}$$

where $Q(i,j)$ is a sample point, the corresponding weight is equal to the Q-mask $M_{Q(i,j)}$ which is equal to 1 for valid Q data and 0 otherwise. Moreover, the mean scattering angle for an angular bin for modeling Mie scattering is,

$$\bar{\Omega}_{n_b} = \frac{\sum_{i,j} M_Q(i,j)\Omega(i,j)}{\sum_{i,j} M_Q(i,j)}. \tag{4}$$

Replacing $\Omega(i,j)$ by $\mu(i,j)$ and $\mu_0(i,j)$ gives the bin averaged cosines of solar zenith angle $\bar{\mu}$ and viewing zenith angle $\bar{\mu}_0$, respectively.

3.3.3 Rayleigh correction

Assuming an atmosphere composed of a cloud layer at the bottom and a Rayleigh layer above it, the Stokes vector $\mathbf{I} = (I, Q, U, V)^T$ referring to the scattering plane is related to the phase matrices of Rayleigh molecules and droplets by the following equation (Diner et al., 2013),

$$\mathbf{I} \approx \frac{\bar{\mu}_0}{4\pi(\bar{\mu}+\bar{\mu}_0)} \frac{E_{0,\lambda}}{d^2} \left\{ e^{-\tau_R(\lambda)(\bar{\mu}^{-1}+\bar{\mu}_0^{-1})} \mathbf{P}_{\text{Mie, Drp}} + (1 - e^{-\tau_R(\lambda)(\bar{\mu}^{-1}+\bar{\mu}_0^{-1})}) \mathbf{P}_{\text{Rayleigh}} \right\} \mathbf{I}_0 + \mathbf{I}_{\text{Unmodeled}}, \tag{5}$$

where $E_{0,\lambda}$ is the exo-atmospheric solar irradiances (cf. 3.2.1.3), d is the Earth-Sun distance in Astronomical Unit (cf. 3.2.1.4), $\mathbf{I}_0 = [1, 0, 0, 0]^T$ for the Sunlight, the first term in the bracket of right-hand-side of Eq. (5) indicates the contribution by single scattering of cloud droplets, and the second term indicated the contribution by single scattering of Rayleigh molecules. $\mathbf{I}_{\text{Unmodeled}}$ accounts for effects excluded by single scattering approximation. Note that the cloudy medium is

assumed semi-infinite and this assumption is compensated for empirically with fitting parameters introduced further on. **P** is a 4 x 4 phase matrix is expressed in the following form,

$$\mathbf{P} = \begin{bmatrix} P_{11,} & P_{12} & 0 & 0 \\ P_{21} & P_{22} & 0 & 0 \\ 0 & 0 & P_{33} & P_{34} \\ 0 & 0 & P_{43} & P_{44} \end{bmatrix}. \tag{6}$$

With the subscripts "R" and "Mie", $\mathbf{P}_R$, and $\mathbf{P}_{Mie}$ denote Rayleigh scattering by molecules and Mie scattering by droplets, respectively, for which $P_{12} = P_{21}$, $P_{34} = -P_{43}$. Moreover, $P_{34} = 0$ for Rayleigh scattering. With the depolarization factor of Rayleigh scattering ($\delta_R = 0.029$, which can be set via "Delta_R" in RCF), the polarized Rayleigh scattering is computed by (Hansen and Travis, 1974),

$$P_{12,\,R} = -\frac{3}{4}\frac{1-\delta_R}{1+\delta_R/2}\sin^2\bar{\Omega}. \tag{7}$$

In addition, the Rayleigh optical depth above the cloud (τ_R) is computed by

$$\tau_R(\lambda) = \tau_{R,tot}\exp(-H_{CT}/H_R). \tag{8}$$

In Eq. (8), the total Rayleigh optical depth $\tau_{R,\,tot}$ at the three AirMSPI polarimetric bands is computed for US standard atmosphere at the sea level according to Bodhaine et al. (1999). Their values are given in Section 6.4 and are fixed during the retrieval. Moreover, the default scale height of the Rayleigh atmosphere H_R is set as 8 km, an altitude where the atmospheric pressure reduces to 1/e of the sea surface. The default cloud-top height is set as H_{CT} = 1 km, a typical value for common stratocumulus clouds off the coast of California. When more accurate information is available, "H_R" and "H_{CT}" can be varied via "HR" and "HCT" in RCF.

Rayleigh scattering and atmospheric attenuation in Eq. (5) need to be removed before fitting observed polarized radiance by P_{12}^{Mie} from droplet scattering. To this end, the data Q is corrected in the following way to get the corrected polarized radiance before retrieval starts [Diner et al., 2013; Bréon and Goloub, 1998):

$$\bar{P}_{12}^{Obs}(\lambda;\bar{\Omega}) = e^{\tau_R(\lambda)(\bar{\mu}^{-1}+\bar{\mu}_0^{-1})}\left[\frac{4\pi(\bar{\mu}+\bar{\mu}_0)}{\bar{\mu}_0 E_{0,\lambda}/d^2}\bar{Q}^{Obs}(\lambda;\bar{\Omega}) - P_{12,\,R}(\lambda;\bar{\Omega})(1-e^{-\tau_R(\bar{\mu}^{-1}+\bar{\mu}_0^{-1})})\right]. \tag{9}$$

Note that $\bar{Q}^{Obs}(\lambda;\bar{\Omega})$ contains both P_{12}^{Mie} as well as the contribution of unmodeled effect via $\mathbf{I}_{Unmodeled}$ in Eq.(5). The latter will be accounted by an empirically terms ($a\lambda$, $b\lambda$, $c\lambda$) to be introduced in the next subsection.

Associated with $\bar{P}_{12}^{\mathrm{Obs}}$, the standard deviation of P_{12}^{Obs} in n_b^{th} angular bin is,

$$\sigma_{n_b}^{\bar{P}_{12}^{\mathrm{Obs}}} = e^{\tau_R(\lambda)\left(\bar{\mu}+\bar{\mu}_0\right)} \frac{4\pi(\bar{\mu}+\bar{\mu}_0)}{\bar{\mu}_0 E_{0,\lambda}/d^2} \sigma_{n_b}^{\bar{Q}^{\mathrm{Obs}}}, \tag{10}$$

which will be used for cost function calculation as well as for retrieval error estimate (cf. 3.3.4 and 3.3.5).

3.3.4 Two-step droplet size retrieval algorithm

As the cloudbow structure of polarized radiance is dominated by single scattering, P_{12}^{Obs} is fit based on single scattering theory, namely with Bréon and Goloub's modeled polarized phase function expressed as (Diner et al., 2013 and Bréon and Goloub, 1998),

$$\bar{P}_{12}^{\mathrm{Model}}(\lambda;\Omega) = a_\lambda P_{12}^{\mathrm{Mie}}(\lambda;\Omega;r_{\mathrm{eff}},v_{\mathrm{eff}}) + b_\lambda \Omega + c_\lambda, \tag{11}$$

where a_λ mainly accounts for cloud coverage fraction, and b_λ and c_λ mainly account for the above-cloud aerosol contributions and gas absorption to the polarized radiance and other unmodeled effects as indicated in Eq.(5), and the polarized phase function P_{12}^{Mie} is dominated by the droplet size distribution parameterized by effective radius (r_{eff}) and effective variance (v_{eff}) assuming a Gamma distribution for the extended cloud in the image.

With the corrected observation (Eq. 9) and the fitting model (Eq. 11), a two-step iterative procedure is designed for droplet size retrieval.

As initialization, we set $a_\lambda = 1$, $b_\lambda = 0$, and $c_\lambda = 0$. Moreover, we interpolate $P_{12,\mathrm{LUT}}^{\mathrm{Mie}}(\lambda;\Omega_{\mathrm{LUT}};r_{\mathrm{eff,\,LUT}},v_{\mathrm{eff,\,LUT}})$ versus gridded scattering angles to get the LUT of $P_{12,\mathrm{LUT}}^{\mathrm{Mie}}(\lambda;\bar{\Omega}_{n_b};r_{\mathrm{eff,\,LUT}},v_{\mathrm{eff,\,LUT}})$ at each binned scattering angle $\bar{\Omega}_{n_b}$ before the iterative process starts.

Step 1: Modify the LUT of P_{12}^{Mie} with (a_λ, b_λ, c_λ) to get $\bar{P}_{12}^{\mathrm{Model}}$ by Eq.(11) and search for the solution of effective radius ($r_{\mathrm{eff,\,LUT}}$) and variance ($v_{\mathrm{eff,\,LUT}}$) whose $\bar{P}_{12}^{\mathrm{Model}}(\lambda;\bar{\Omega}_{n_b};r_{\mathrm{eff,\,LUT}},v_{\mathrm{eff,\,LUT}})$ fits $P_{12}^{\mathrm{Obs}}(\lambda;\bar{\Omega}_{n_b})$ with smallest reduced χ^2 error, which is defined as:

$$\chi^2 = \left[\sum_{i=1}^{N_\lambda} N_{\mathrm{b,\,Re}}(\lambda_i) - N_{\mathrm{Par}}\right]^{-1} \sum_{i=1}^{N_\lambda} \sum_{n_b=1}^{n_b=N_{\mathrm{b,\,Re}}} \left[\frac{\bar{P}_{12}^{\mathrm{Obs}}(\lambda_i;\bar{\Omega}_{n_b}) - P_{12}^{\mathrm{Model}}(\lambda_i;\bar{\Omega}_{n_b};r_{\mathrm{eff}},v_{\mathrm{eff}})}{\sigma_{n_b}^{\bar{P}_{12}^{\mathrm{Obs}}}}\right]^2, \tag{12}$$

where $N_{\mathrm{b,Re}}$ is the number of angular bins in $\Omega_{\mathrm{min,\,re}} \le \Omega \le \Omega_{\mathrm{max,\,re}}$ and N_{Par} is the number of parameters to retrieve ($N_{\mathrm{Par}} = 11$ in this ATBD, including 2 parameters, r_{eff} and v_{eff},, for droplet size distribution and 9 parameters, a_λ, b_λ and c_λ, for the three polarimetric bands). Assuming the index M is associated with minimum χ^2 value, then the indices L = M-1 and R = M+1 are

associated with the two neighbor solutions of effective radius ($r_{\text{eff, LUT, L}}$, $r_{\text{eff, LUT, R}}$) around $r_{\text{eff, LUT,M}}$. A parabolic fit of residues is invoked to determine the optimal effective radius of $r_{\text{eff},n}$ at the current iterative step n, namely for $x = r_{\text{eff}}$, we have

$$x_n = \frac{(x^2_{\text{LUT, L}} - x^2_{\text{LUT, M}}) - t(x^2_{\text{LUT, M}} - x^2_{\text{LUT, R}})}{2[(x_{\text{LUT, L}} - x_{\text{LUT, M}}) - t(x_{\text{LUT, M}} - x_{\text{LUT, R}})]}, \tag{13}$$

with

$$t = \frac{\chi^2_{\text{LUT, L}} - \chi^2_{\text{LUT, M}}}{\chi^2_{\text{LUT, M}} - \chi^2_{\text{LUT, R}}}, \tag{14}$$

where $\chi^2_{\text{LUT, L}}$, $\chi^2_{\text{LUT, M}}$ and $\chi^2_{\text{LUT, R}}$ are the reduced χ^2 residues at $x_{\text{LUT, L}}$, $x_{\text{LUT, M}}$ and $x_{\text{LUT, R}}$, respectively. The residue at $x_n = r_{\text{eff},n}$ is then evaluated by,

$$\chi^2_n = \chi^2_{\text{LUT,L}} - \frac{(\chi^2_{\text{LUT,L}} - \chi^2_{\text{LUT, M}})(x_{\text{LUT,L}} - x_n)^2}{(x_{\text{LUT,L}} - x_n)^2 - (x_{\text{LUT, M}} - x_n)^2}. \tag{15}$$

Next, at the two neighboring grids of variance around the LUT solution of variance ($v_{\text{eff, LUT, Mv}}$) namely $v_{\text{eff, LUT, Lv}}$ and $v_{\text{eff, LUT, Rv}}$ ($L_v = M_v$-1 and $R_v = M_v$+1) interpolation over effective radius is used to get the residues $\chi^2_{\text{veff, Lv}}$ and $\chi^2_{\text{veff, Rv}}$ at $r_{\text{eff},n}$ determined from Step 1. Knowing ($v_{\text{eff, LUT, Lv}}$, $\chi^2_{\text{veff, Lv}}$), ($v_{\text{eff, LUT, Mv}}$, $\chi^2_{\text{veff, Mv}}$), and ($v_{\text{eff, LUT, Rv}}$, $\chi^2_{\text{veff, Rv}}$), the parabolic fitting using Eqs.(13)-(15) is repeated for $x = v_{\text{eff}}$ to get the optimal effective variance $v_{\text{eff},n}$ and fitting error χ^2_n at the current iterative step n.

Knowing the iterative solution ($r_{\text{eff},n}$, $v_{\text{eff},n}$), the polarized phase function $P_{12}^{\text{Mie}}(\lambda;\bar{\Omega}_i;r_{\text{eff,R}},v_{\text{eff},n})$ and modeled polarization $P_{12}^{\text{Model}}(\lambda;\bar{\Omega}_i;r_{\text{eff,R}},v_{\text{eff},n})$ can be evaluated by invoking the following two steps of interpolation:

1): at the fixed grid value of $r_{\text{eff,L}}$, we have two adjacent LUT grids that bound $v_{\text{eff},n}$ and then linearly interpolating them to get P_{12}^{Mie} ($r_{\text{eff, L}}$, $v_{\text{eff},n}$). Namely assuming $x_L = v_{\text{eff, L}}$, $x_R = v_{\text{eff, R}}$ are the two points bounding $x = v_{\text{eff},n}$, with $x \geq x_L$ and $x < x_R$, then at an arbitrary scattering angle Ω_i, we have $P_{12}^{\text{Mie}}(\lambda;\bar{\Omega}_i;r_{\text{eff,L}},v_{\text{eff},n}) = P_{12}^{\text{Mie}}(\lambda;\bar{\Omega}_i;x)$, which is evaluated from linear polarization, namely,

$$P_{12}^{\text{Mie}}(\lambda;\bar{\Omega}_i;x) = P_{12}^{\text{Mie}}(\lambda;\bar{\Omega}_i;x_L) + \frac{P_{12}^{\text{Mie}}(\lambda;\bar{\Omega}_i;x_R) - P_{12}^{\text{Mie}}(\lambda;\bar{\Omega}_i;x_L)}{x_R - x_L}(x - x_{\text{LUT,L}}) \tag{16}$$

Then we have $P_{12}^{\text{Model}}(\lambda;\bar{\Omega}_i;r_{\text{eff,L}},v_{\text{eff},n}) = a_\lambda P_{12}^{\text{Mie}}(\lambda;\bar{\Omega}_i;r_{\text{eff,L}},v_{\text{eff},n}) + b_\lambda\bar{\Omega}_i + c_\lambda$ referring to Eq.(11).

The same procedure is applied to get $P_{12}^{\mathrm{Model}}(\lambda;\bar{\Omega}_i;r_{\mathrm{eff,R}},v_{\mathrm{eff},n})$ for the fixed grid value $r_{\mathrm{eff,R}}$;

2): getting $P_{12}^{\mathrm{Mie}}(\lambda;\bar{\Omega}_i;r_{\mathrm{eff},n},v_{\mathrm{eff},n})$ and then $P_{12}^{\mathrm{Model}}(\lambda;\bar{\Omega}_i;r_{\mathrm{eff},n},v_{\mathrm{eff},n})$ by repeating the linear interpolation (Eq.(16)) over effective radius (with $x = r_{\mathrm{eff},n}$ and fixed value $r_{\mathrm{eff},n}$), using $P_{12}^{\mathrm{Model}}(\lambda;\bar{\Omega}_i;r_{\mathrm{eff,L}},v_{\mathrm{eff},n})$ and $P_{12}^{\mathrm{Model}}(\lambda;\bar{\Omega}_i;r_{\mathrm{eff,R}},v_{\mathrm{eff},n})$ obtained from the above step.

Then at the iterative solution ($r_{\mathrm{eff},n}$, $v_{\mathrm{eff},n}$), the Chi-square fitting residue χ_n^2 is updated by substituting $P_{12}^{\mathrm{Model}}(\lambda;\bar{\Omega}_i;r_{\mathrm{eff},n},v_{\mathrm{eff},n})$ into Eq.(12).

Step 2: with ($r_{\mathrm{eff},n}$, $v_{\mathrm{eff},n}$) determined from Step 1, the following linear system of equations is solved for each wavelength to update x=(a_λ, b_λ, c_λ)$^{\mathrm{T}}$:

$$\mathbf{x} = \mathbf{A}^{-1}\mathbf{B}, \tag{17}$$

with

$$\mathbf{A} = \begin{bmatrix} P_{12}^{\mathrm{Mie}}(\lambda;\bar{\Omega}_1;r_{\mathrm{eff},n},v_{\mathrm{eff},n}) & \bar{\Omega}_1 & 1 \\ P_{12}^{\mathrm{Mie}}(\lambda;\bar{\Omega}_2;r_{\mathrm{eff},n},v_{\mathrm{eff},n}) & \bar{\Omega}_2 & 1 \\ \vdots & \vdots & \vdots \\ P_{12}^{\mathrm{Mie}}(\lambda;\bar{\Omega}_{N_\mathrm{b}};r_{\mathrm{eff},n},v_{\mathrm{eff},n}) & \bar{\Omega}_{N_\mathrm{b}} & 1 \end{bmatrix}, \text{ and } \mathbf{B} = \begin{pmatrix} \bar{P}_{12}^{\mathrm{Obs}}(\lambda;\bar{\Omega}_1) \\ \bar{P}_{12}^{\mathrm{Obs}}(\lambda;\bar{\Omega}_2) \\ \vdots \\ \bar{P}_{12}^{\mathrm{Obs}}(\lambda;\bar{\Omega}_{N_\mathrm{b}}) \end{pmatrix} \tag{18}$$

where $P_{12}^{\mathrm{Mie}}(\lambda;\bar{\Omega}_1;r_{\mathrm{eff},n},v_{\mathrm{eff},n})$ is evaluated from the interpolation in Step 1 retrieval.

As the above system is over-determined, (a_λ, b_λ, c_λ) is indeed the linear least-square solution to the minimization of $\|\mathbf{B}-\mathbf{Ax}\|_2$. Among many existing numerical methods, we used the LAPACK solver (Anderson et al., 1999) for Eq.(18).

The above Step 1 and Step 2 are repeated until the difference between two different successive solutions are smaller than criterion values $\varepsilon_{r,\mathrm{c}}$ and $\varepsilon_{v,\mathrm{c}}$ for effective radius and variance respectively, namely when both of the following criterions of convergence are met:

$$|r_{\mathrm{eff},n} - r_{\mathrm{eff},n-1}|/r_{\mathrm{eff},n-1} \le \varepsilon_{r,\mathrm{c}}, \tag{19}$$

$$|v_{\mathrm{eff},n} - v_{\mathrm{eff},n-1}|/v_{\mathrm{eff},n-1} \le \varepsilon_{v,\mathrm{c}}. \tag{20}$$

Here $\varepsilon_{r,\mathrm{c}}$ and $\varepsilon_{v,\mathrm{c}}$ are specified via "Eps_reff" and "Eps_veff" respectively, via the RCF.

The retrieval is marked as successful with retrieval quality indicator RQI = 1 when (a) both effective radius and variance are within their bounds, namely $\min(r_{\mathrm{eff,LUT}}) < r_{\mathrm{eff},n} < \max(r_{\mathrm{eff,LUT}})$ and $\min(v_{\mathrm{eff,LUT}}) < v_{\mathrm{eff},n} < \max(v_{\mathrm{eff,LUT}})$, and (b) the Chi-square fitting error is smaller than the criterion value specified in RCF via "Chi_Cri".

However, if a) is violated, then retrieval fails with RQI = 2; and
if b) is violated, the retrieval fails with RQI = 3.

In addition, the retrieval fails with RQI = 4 when retrieval exceeds the maximum number of iterations without convergence. The maximum number of iterations is specified in RCF via "N_Max_Ite". Its default value is set to be 15 according to our retrieval test.

As RQI = 1, 2, 3, and 4, the iterative solution ($r_{\text{eff},n}, v_{\text{eff},n}$) is used as the optimized solution and output to the retrieval product together with the modeled polarization $P_{12}^{\text{Model}}(\lambda;\bar{\Omega}_i;r_{\text{eff},n},v_{\text{eff},n})$ and fitting error χ_n^2, namely $r_{\text{eff, opt}} = r_{\text{eff},n}$, $v_{\text{eff, opt}} = v_{\text{eff},n}$, $P_{12,\text{opt}}^{\text{Model}} = P_{12}^{\text{Model}}(\lambda;\bar{\Omega}_i;r_{\text{eff},n},v_{\text{eff},n})$, and $\chi_{\text{opt}}^2 = \chi_n^2$.

Note that retrieval is not implemented when the number of signals in a spectral band is less than three or the total number of signals from all bands is less than the total number in retrieval (namely $N_{\text{Par}} = 11$). In the former case, (a_λ, b_λ, c_λ) alone cannot be derived. In the latter case, (r_{eff}, v_{eff}) together with (a_λ, b_λ, c_λ) for the three polarimetric bands cannot be derived. Whatever the case, RQI is set to be 5. Moreover, without applying any cloud mask algorithm, the failure of retrieval with RQI = 3 can be because the scene is only partially covered by cloud and/or surface reflection have significant contribution to observed Q signals that is not well modeled by a droplet size distribution.

3.3.5 Retrieval of 1D-RT based cloud optical depth

Without accounting for the 3D radiative effects [e.g., Davis et al. 1997] and assuming homogeneous droplet size distribution throughout the cloud layer, the 1D-RT based cloud optical depth is retrieved at each cloudy pixel using the radiance at the three polarimetric bands. The valid pixels are identified as those with mask values for I and Q at all polarimetric bands being unity, and cloudy (identified from I at 660 nm, cf. Section 3.3.1), namely,

$$\begin{aligned}&\text{I.mask(470 nm) x I.mask(660 nm) x I.mask(865 nm) x}\\&\text{Q.mask(470 nm) x Q.mask(660 nm) x Q.mask(865 nm) x (I(660 nm)>I}_{\text{threshold}}\text{) = 1.}\end{aligned} \tag{21}$$

Then for j^{th} band and k^{th} pixel which has viewing geometry $\Lambda_{k,j} = (\mu,\mu_0;\phi-\phi_0)_{k,j}$, we search for an optimized pixel-scale cloud optical depth τ_{COD} which corresponds to the modeled radiance $L^{\text{Model}}(\tau_\lambda;\Lambda_k;r_{\text{eff, opt}},v_{\text{eff, opt}})$ that fit observations $L^{\text{Obs}}(\lambda_j;\Lambda_{k,j})$ with the smallest reduced chi-square error defined as:

$$\chi_{L,k}^2 = (N_\lambda - 1)^{-1}\sum_{j=1}^{N_\lambda}\left[\frac{L^{\text{Obs}}(\lambda_j;\Lambda_{k,j}) - L^{\text{Model}}(\tau_{\lambda_j};\Lambda_{k,j})}{\delta_L}\right]^2, \tag{22}$$

where δ_L is the relative error of radiance (adopted as 1.5% in this study). Note that the term "radiance" used in cloud optical depth retrieval is normalized by Earth-Sun distance and solar irradiance. In other words, we assume unit solar irradiance and Earth-Sun distance. In practical implementation, parabolic fitting is used to determine the optimized cloud optical depth, namely in Eqs.(13-14), the index M is associated with minimum χ^2 value, then the indices L = M-1 and R = M+1 are associated with the two neighbor solutions of cloud optical depth ($\tau_{LUT,L}$, $\tau_{LUT,R}$) around $\tau_{LUT,M}$. To evaluate $L^{Model}(\tau_{\lambda_j};\Lambda_{k,j})$, the following three steps are taken:

Step 1: use one-dimensional linear interpolation over solar zenith angle to get the radiance look up table for the cloud scene with spatially and spectrally averaged solar zenith angle $\bar{\theta}_0$, namely $L(\tau_{\lambda_j};\theta_k,\bar{\theta}_0;\phi_k-\phi_{0,k})$;

Step 2: get the one-dimensional look up table (radiance versus cloud optical depth) at the optimized droplet size distribution, namely $L^{Model}(\tau_{\lambda_j};\Lambda_{k,j})$ at ($r_{eff,opt}$, $v_{eff,opt}$). This is evaluated by taking the following two sub-steps:

1): at the fixed grid value of $r_{eff,L}$, we have two adjacent LUT grids that bound $v_{eff,opt}$ and then linearly interpolating them to get $L(\tau_\lambda;r_{eff,L},v_{eff,n})$. Namely assuming $x_L = v_{eff,L}$, $x_R = v_{eff,R}$ are the two points bounding $x = v_{eff,n}$, with $x \geq x_L$ and $x < x_R$, then at an arbitrary incidence and viewing geometry $\Lambda_{k,j} = (\mu,\mu_0;\phi-\phi_0)_{k,j}$, we have $L(\tau_{\lambda_j};\Lambda_{k,j};r_{eff,L},v_{eff,n})$ evaluated from linear polarization, namely,

$$L^{Model}(\tau_{\lambda_j};\Lambda_{k,j};x) = L^{Model}(\tau_{\lambda_j};\Lambda_{k,j};x_L) + \frac{L^{Model}(\tau_{\lambda_j};\Lambda_{k,j};x_R) - L^{Model}(\tau_{\lambda_j};\Lambda_{k,j};x_L)}{x_R - x_L}(x - x_L) \quad (23)$$

The same procedure is applied to get $L(\tau_{\lambda_j};\Lambda_{k,j};r_{eff,R},v_{eff,n})$ for the fixed grid value $r_{eff,R}$;

2): getting $L(\tau_{\lambda_j};\Lambda_{k,j};r_{eff,n},v_{eff,n})$ by repeating the linear interpolation (Eq.(23)) over effective radius (with $x = r_{eff,n}$ and fixed value $r_{eff,n}$), using $L(\tau_{\lambda_j};\Lambda_{k,j};r_{eff,L},v_{eff,n})$ and $L(\tau_{\lambda_j};\Lambda_{k,j};r_{eff,R},v_{eff,n})$ obtained from the above step;

Step 3: using two-dimensional linear interpolation over viewing angle θ and azimuthal angle ϕ-ϕ_0 of an arbitrary (k^{th}) pixel to get the local look up table, namely, $L(\tau_{\lambda_j};\theta_k,\bar{\theta}_0;\phi_k-\phi_{0,k})$, or $L(\tau_{\lambda_j};\Lambda_{k,j})$ in Eq. (22).

After retrieving cloud optical depth over all cloudy pixels, mean value ($\tau_{COD,mean}$) and standard deviation ($\sigma_{\tau COD}$) of cloud optical depth are calculated and delivered as the product.

3.3.6 Retrieval uncertainties

a) droplet size parameters

The retrieval error of j^{th} parameter x_j (j = 1 or 2 for $\mathbf{x}$ = [r_{eff}, v_{eff}, a_{470}, a_{660}, a_{865}, b_{470}, b_{660}, b_{865}, c_{470}, c_{660}, c_{865}]) is estimated by [Xu et al. 2017],

$$\Delta_j^2 = \left\{ \text{diag}[(\mathbf{J}^{\text{T}}\mathbf{W}\mathbf{J})^{-1} + \mathbf{X}_{\text{bias}}\mathbf{X}_{\text{bias}}^{\text{T}}] \right\}_j, \tag{24a}$$

and

$$\mathbf{X}_{\text{bias}} = \left(\mathbf{J}^{\text{T}}\mathbf{W}\mathbf{J}\right)^{-1}\left[\mathbf{J}^{\text{T}}\mathbf{W}(\mathbf{Y}^{\text{Obs}} - \mathbf{Y}^{\text{Model}})\right], \tag{24b}$$

where the observation column vector contains observations in all polarimetric bands, namely, $\mathbf{Y}^{\text{Obs}} = \left[\bar{P}_{12}^{\text{Obs}}(\lambda_1;\bar{\Omega}_{n_b});\bar{P}_{12}^{\text{Obs}}(\lambda_2;\bar{\Omega}_{n_b});\bar{P}_{12}^{\text{Obs}}(\lambda_3;\bar{\Omega}_{n_b})\right]$, the modeling column vector contains modeled results in all spectral bands with the optimized solution, namely, $\mathbf{Y}^{\text{Model}} = \left[\bar{P}_{12}^{\text{Model}}(\lambda_1;\bar{\Omega}_{n_b};r_{\text{eff, opt}},v_{\text{eff, opt}});\bar{P}_{12}^{\text{Model}}(\lambda_2;\bar{\Omega}_{n_b};r_{\text{eff, opt}},v_{\text{eff, opt}});\bar{P}_{12}^{\text{Model}}(\lambda_3;\bar{\Omega}_{n_b};r_{\text{eff, opt}},v_{\text{eff, opt}})\right]$, the weighting matrix $\mathbf{W}$ is diagonal with $W_{ii} = 1/w_i^2$, with w_i being the standard error of measurement (here we assume $w_i = \sigma_i$, and σ is given in Eq. (3)), $\mathbf{J}^{\text{T}}$ is transpose of the Jacobian matrix $\mathbf{J}$ with components at the three AirMSPI wavelengths, namely,

$$\mathbf{J} = \begin{bmatrix} \mathbf{J}_1(\lambda_1) & \mathbf{J}_2(\lambda_1) & \mathbf{0} & \mathbf{0} \\ \mathbf{J}_1(\lambda_2) & \mathbf{0} & \mathbf{J}_2(\lambda_2) & \mathbf{0} \\ \mathbf{J}_1(\lambda_3) & \mathbf{0} & \mathbf{0} & \mathbf{J}_2(\lambda_3) \end{bmatrix}, \tag{25a}$$

where "**0**" denotes the 3x3 null matrix,

$$\mathbf{J}_1(\lambda_n) = \begin{bmatrix} a_{\lambda_n}\dfrac{\partial P_{12}^{\text{Mie}}(\lambda_n;\bar{\Omega}_1)}{\partial r_{\text{eff}}} & a_{\lambda_n}\dfrac{\partial P_{12}^{\text{Mie}}(\lambda_n;\bar{\Omega}_1)}{\partial v_{\text{eff}}} \\ a_{\lambda_n}\dfrac{\partial P_{12}^{\text{Mie}}(\lambda_n;\bar{\Omega}_2)}{\partial r_{\text{eff}}} & a_{\lambda_n}\dfrac{\partial P_{12}^{\text{Mie}}(\lambda_n;\bar{\Omega}_2)}{\partial v_{\text{eff}}} \\ \cdots & \cdots \\ a_{\lambda_n}\dfrac{\partial P_{12}^{\text{Mie}}(\lambda_n;\bar{\Omega}_{N_b})}{\partial r_{\text{eff}}} & a_{\lambda_n}\dfrac{\partial P_{12}^{\text{Mie}}(\lambda_n;\bar{\Omega}_{N_b})}{\partial v_{\text{eff}}} \end{bmatrix}, \tag{25b}$$

and

$$\mathbf{J}_2(\lambda_n) = \begin{bmatrix} P_{12}^{\text{Mie}}(\lambda_n;\bar{\Omega}_1) & \bar{\Omega}_1 & 1 \\ P_{12}^{\text{Mie}}(\lambda_n;\bar{\Omega}_2) & \bar{\Omega}_2 & 1 \\ \cdots & \cdots & \cdots \\ P_{12}^{\text{Mie}}(\lambda_n;\bar{\Omega}_{N_b}) & \bar{\Omega}_{N_b} & 1 \end{bmatrix}. \tag{25c}$$

In Eq.(25b), the derivative of the polarized phase function with respect to x (x being either r_{eff} or

v_{eff}), namely $\frac{\partial P_{12}^{\text{Mie}}(\lambda;\bar{\Omega}_i)}{\partial x}$, is approximated by finite difference method using the polarized phase functions at two neighbor grids around the LUT solution ($r_{\text{eff, LUT}}$, $v_{\text{eff, LUT}}$), namely

$$\frac{\partial P_{12}^{\text{Mie}}(\lambda;\bar{\Omega}_i;x)}{\partial x} = \frac{P_{12}^{\text{Mie}}(\lambda;\bar{\Omega}_i;x_{\text{R}}) - P_{12}^{\text{Mie}}(\lambda;\bar{\Omega}_i;x_{\text{L}})}{x_{\text{R}} - x_{\text{L}}}, \tag{26}$$

where as a function of scattering angles of data ($\bar{\Omega}_i$), $P_{12}^{\text{Mie}}(\bar{\Omega}_i)$ is obtained by interpolating the LUT table $P_{12,\text{LUT}}^{\text{Mie}}(\bar{\Omega}_{\text{LUT}})$. $P_{12}^{\text{Mie}}(\bar{\Omega}_i)$ is indeed implemented before retrieval starts (cf. Section 3.3.4). Moreover, when calculating $\frac{\partial P_{12}^{\text{Mie}}(\lambda;\bar{\Omega}_i;x)}{\partial x}$ for $x = r_{\text{eff}}$, v_{eff} is fixed to be $v_{\text{eff, LUT}}$; when calculating $\frac{\partial P_{12}^{\text{Mie}}(\lambda;\bar{\Omega}_i;x)}{\partial x}$ for $x = v_{\text{eff}}$, r_{eff} is fixed to be $r_{\text{eff, LUT}}$.

Equation (24) means the j^{th} term of the diagonal of matrix $[\mathbf{J}^{\text{T}}\mathbf{W}\mathbf{J}]^{-1}$ contains the retrieval error of j^{th} parameter in the solution vector $\mathbf{x}$.

b) 1D-RT based cloud optical depth

Invoking the relationship between cloud optical depth (τ) and droplet concentration, extinction cross-section (C_{ext}) and cloud layer depth (H), $\tau = C_n C_{\text{ext}} H$, the retrieval error is evaluated by use of the chain rule,

$$\left(\frac{\Delta\tau}{\tau}\right)^2 = \tau^2\left(\frac{\Delta C_n}{C_n}\right)^2 + \left(\frac{\tau}{C_{\text{ext}}}\right)^2\left(\frac{\partial C_{\text{ext}}}{\partial r_{\text{eff}}}\right)^2 \Delta r_{\text{eff}}^2 + \left(\frac{\tau}{C_{\text{ext}}}\right)^2\left(\frac{\partial C_{\text{ext}}}{\partial v_{\text{eff}}}\right)^2 \Delta v_{\text{eff}}^2, \tag{27}$$

where C_{ext} for the optimized size distribution ($r_{\text{eff,opt}}$, $v_{\text{eff,opt}}$) is evaluated from two-dimensional linear interpolation over LUT grids of r_{eff} and v_{eff} and Δr_{eff} and Δv_{eff} are as evaluated in Section 3.3.6a. Equation (27) is equivalent to the following form for implementation,

$$\left(\frac{\Delta\tau_\lambda}{\tau_\lambda}\right)^2 = \tau_\lambda^2\left(\frac{\Delta C_n H}{C_n H}\right)^2 + \left(\frac{\tau_{660\text{nm}}}{C_{\text{ext, 660nm}}}\right)^2\left(\frac{\partial C_{\text{ext},\lambda}}{\partial r_{\text{eff}}}\right)^2 \Delta r_{\text{eff}}^2 + \left(\frac{\tau_{660\text{nm}}}{C_{\text{ext, 660nm}}}\right)^2\left(\frac{\partial C_{\text{ext},\lambda}}{\partial v_{\text{eff}}}\right)^2 \Delta v_{\text{eff}}^2, \tag{28}$$

where the retrieval error $\Delta\tau_{660\text{nm}}$ is evaluated by Eq.(24), in which relative uncertainty of radiance measurement is used for evaluating weighting matrix $\mathbf{W}$ and the Jacobian matrix $\mathbf{J}$ is written as

$$\mathbf{J} = \left[\begin{array}{ccc} \frac{\partial L_{470\text{nm}}^{\text{Model}}}{\partial(C_n H)} & \frac{\partial L_{660\text{nm}}^{\text{Model}}}{\partial(C_n H)} & \frac{\partial L_{865\text{nm}}^{\text{Model}}}{\partial(C_n H)} \end{array}\right]^{\text{T}}, \tag{29}$$

where $\frac{\partial L_{865\text{nm}}^{\text{Model}}}{\partial(C_n H)}$ is evaluated using finite difference method, namely,

$$\frac{\partial L_{\lambda}^{\text{Model}}}{\partial(C_n H)} = \frac{L_{865\text{nm}}^{\text{Model}}(\tau_{\lambda,\text{R}}) - L_{865\text{nm}}^{\text{Model}}(\tau_{\lambda,\text{L}})}{(\tau_{\lambda,\text{R}} - \tau_{\lambda,\text{L}})/C_{\text{ext},\lambda}}. \tag{30}$$

3.3.7 Retrieval products

The droplet size retrieval product includes:

1) Retrieval quality indicator RQI;
2) Optimized effective radius $r_{\text{eff, opt}}$ and its uncertainty;
3) Optimized effective variance $v_{\text{eff, opt}}$ and its uncertainty;
4) Optimized fitting parameters ($a_{\lambda,\text{ opt}}$, $b_{\lambda,\text{ opt}}$, $c_{\lambda,\text{ opt}}$) and their uncertainties;
5) Corrected polarization signals ("$\bar{P}_{12}^{\text{Obs}}$" in Eq. (9)) with standard deviation ("$\sigma^{\text{P}^{\text{Obs}}}$" in Eq. (10)) and modeled results ("$P_{12,\text{ opt}}^{\text{Model}}$" in Eq. (11)) in the scattering angles $\Omega_{\text{Min}} \le \Omega \le \Omega_{\text{Max}}$, using the optimization solution;
6) Reduced Chi-square residue (χ^2_{opt} in Eq.(12)) which corresponds to fitting polarized radiance over the scattering angular bins $\Omega_{\text{min, re}} \le \Omega \le \Omega_{\text{max, re}}$;
7) Pixel scale cloud optical depth (τ_{COD}) at 470, 660 and 865 nm;
8) Uncertainty of pixel scale cloud optical depth ($\Delta\tau_{\text{COD}}$ in Eq.(28)) at 470, 660 and 865 nm;
9) Image averaged cloud optical depth value ($\tau_{\text{COD,mean}}$) and standard deviation ($\sigma_{\tau_{\text{COD}}}$) at 470, 660 and 865 nm;
10) Modeled radiance ($L^{\text{Model}}(\tau_{\lambda_j};\Lambda_{k,j})$) at 470, 660 and 865 nm at valid pixels where retrieval is performed;
11) Observed radiance ($L^{\text{Obs}}(\tau_{\lambda_j};\Lambda_{k,j})$) at 470, 660 and 865 nm at valid pixels where retrieval is performed;
12) Pixel resolved reduced Chi-square residue from radiance fit ($\chi^2_{L,\text{opt}}$ in Eq.(22));
13) Latitude and longitude of all valid pixels where retrieval is performed.

But for RQI = 5, only "RQI" and the corrected polarization signal "P_Obs" ("$\bar{P}_{12}^{\text{Obs}}$" in Eq. (9)) with standard deviation "Std_P_Obs" ("$\sigma^{\text{P}^{\text{Obs}}}$" in Eq. (10)) are output.

As indicated in Table 1, the following ancillary parameters are also included in the product:

1) Name of the L1B2 input file;
2) Acquisition start and end time;
3) Upper left latitude and longitude of cloud image;
4) Upper right latitude and longitude of cloud image;
5) Lower left latitude and longitude of cloud image;
6) Lower right latitude and longitude of cloud image;

7) Names of radiometric and vicarious calibration files.

4 ASSUMPTIONS AND LIMITATIONS

4.1 ASSUMPTIONS

The following assumptions are made for retrieving cloud-top droplet size distribution:

(1) Horizontally and vertically uniform distribution of droplet size distribution of top part of the cloud, which is characterized by Gamma distribution via effective radius and effective variance.

(2) The two-parameter (effective radius and effective variance) constrained droplet size distribution is representative of the real cloud-top droplet size distribution profile in modeling the observed cloudbow polarization.

(3) Pure water droplets with the refractive index given by Daimon and Masumura (2007) for the temperature 19 ºC.

(4) All unmodeled effects, including cloud heterogeneity, above-cloud aerosols, trace gas absorption, etc. are accommodated by the empirical terms a_λ, b_λ, and c_λ in Eq. (11).

The following assumptions are made for retrieving cloud optical depth:

(1) The cloud-top droplet size distribution retrieved using polarized radiance in cloudbow region is valid over the whole cloud image.

(2) There are no vertical and horizontal variations of the cloud droplet size distribution.

(3) 3D radiative effects [e.g., Davis et al. 1997] are omitted.

4.2 LIMITATIONS

The following limitations apply to the cloud droplet retrievals:

(1) When there is large fraction of cloud-free or glint pixels over the image, retrievals may be associated with ocean and terrain reflectance effects rather than cloud effects. In this case the retrieval may fail with RQI > 1 and a large Chi-square fitting error.

(2) When clouds are not strictly stratocumulus or when liquid droplet particles are mixed with ice-crystal particles, a number of retrievals can fail as the cloudbow structure may be biased and empirical parameters in Eq. (11) cannot well accommodate these effects.

(3) The modeling errors of Eq. (11) are not fully accounted in the error analysis. Moreover, the standard deviations of Q in all angular bins are treated as random errors in retrieval error analysis for effective radius and effective various. Thus, the retrieval uncertainties obtained from Eq. (24) have limitations in representing the retrieval error in strict sense.

(4) In the presence of spatial heterogeneity of droplet sizes and concentration, the

1D RT based cloud optical depth retrieval as well as the polarization based droplet size retrieval may be subjected to bias. These effects are a topic of ongoing research.

(5) The identification of cloudy pixels utilizes the radiometric contrast at 660 nm between clouds and an ocean background. Land surface, often significantly brighter than ocean, may be misinterpreted for a cloud.

5 REFERENCES

[1] Anderson, E., et al. *LAPACK Users' Guide*. Third Edition. SIAM, Philadelphia (1999). (Least square solution solver: http://www.netlib.org/lapack/lug/node27.html)

[2] Alexandrov, M. D., et al. Accuracy assessments of cloud droplet size retrievals from polarized reflectance measurements by the research scanning polarimeter. Remote Sens. Environ. 125, 92-111, 2012.

[3] Bodhaine, B. A., et al. On Rayleigh optical depth calculations. J. Atmos. Oceanic Technol. 16, 1854-1861, 1999.

[4] Bréon, F.-M. and P. Goloub. Cloud droplet effective radius from spaceborne polarization measurements, Geophys. Res. Lett. 25,1879-1882, 1998.

[5] Daimon, M. and A. Masumura. Measurement of the refractive index of distilled water from the near-infrared region to the ultraviolet region. Appl. Opt. 46, 3811-3820, 2007.

[6] Davis, A., A. Marshak, R.F. Cahalan, and W.J. Wiscombe. The Landsat scale-break in stratocumulus as a three-dimensional radiative transfer effect, Implications for cloud remote sensing. J. Atmos. Sci. 54, 241-260, 1997.

[7] Diner, D. J., et al. Dual photoelastic modulator-basedpolarimetric imaging concept for aerosol remote sensing. Appl. Opt. 46, 8428-8445, 2007.

[8] Diner, D. J., et al. The Airborne Multiangle SpectroPolarimetric Imager (AirMSPI): a new tool for aerosol and cloud remote sensing. Atmos. Meas. Tech. 6, 2007-2025, 2013.

[9] Hansen, J. E., and L. D. Travis. Light scattering in planetary atmospheres. Space Sci. Rev., 16, 527-610 (1974).

[10] Shen, J. and X. Cai. Algorithm of numerical calculation on Lorentz Mie theory. PIERS Online 1, 691-694, 2005.

[11] Wehrli, C. Extraterrestrial solar spectrum, Publication no. 615, Physikalisch-Meteorologisches Observatorium + World Radiation Center (PMO/WRC) Davos Dorf, Switzerland, July 1985.

[12] Xu, F., et al. Joint retrieval of aerosol and water-leaving radiance from multispectral, multiangular and polarimetric measurements over ocean, Atmos. Meas. Tech., 9, 2877-2907, 2016.

[13] Xu, F., et al. Coupled retrieval of liquid water cloud and aerosol above cloud properties using the Airborne Multiangle SpectroPolarimetric Imager (AirMSPI). J. Geophys. Res., in review (2017).

6 APPENDIX

6.1 Refractive index of droplets

Table 3: Refractive index of water droplet in 470, 660 and 865 nm bands at the temperature T = 19ºC. Interpolation was used to get the values at the AirMSPI wavelengths.

Wavelength (nm)	Real part of refr. index	Imaginary part of refr. index
470	1.338470	0
660	1.331511	0
865	1.327615	0

6.2 Grids of effective radius in look-up-table

For Mie scattering property calculation, the range of effective radius (r_{eff}) is set to be $5 \leq r_{eff} \leq 20$ μm to cover a typical range of droplet size, and the grid values have the increment 0.05. There are 301 grids for r_{eff} in total. Such a setting is same as that used for droplet size retrieval in Alexandrov et al. (2012). For building the cloud optical depth look-up-table, there are 31 grids in the same size range for r_{eff} in total, namely the step increment is 0.5.

6.3 Grids of effective variance in look-up-table

For Mie scattering property calculation, the effective variance (v_{eff}) in our LUT starts with values of 0.001, 0.004, and 0.007. Then it has the regular increment of 0.0025 from 0.01 to the maximum 0.4. There are 160 grids for v_{eff} in total. Such a setting is similar to that used in Alexandrov et al. (2012). But the upper bound of our v_{eff} is larger by 0.05. Moreover, we start with smaller values of variance as they are retrieved from some of AirMSPI cloudbow observations. For building the cloud optical depth look-up-table, there are 17 grids in the same range of v_{eff} in total, with the step increment changed to 0.03.

6.4 Angular resolution

The scattering angular resolution is 0.25 degree for Mie scattering phase function calculation calculated from 0° to 180°. For retrieving cloud optical depth, the look-up-table is developed for a) viewing angular resolution 1° from 0 to 90° so that that total number of grids are 91, b) solar zenith angular resolution 5° from 0° to 85° degree so that that total number of grids are 19, and azimuthal angular resolution 2° from 0° to 180° so that that total number of grids are 91.

6.5 Cloud optical depth grids

For the 1D look-up-table of radiance versus cloud optical depth, 16 cloud optical depth grids are set from 0.5 to 500, with the geometric regression factor ~1.58.

6.6 Rayleigh optical depth at AirMSPI polarimetric bands

Table 4: Rayleigh optical depth ($\tau_{R,tot}$) calculated for U.S. standard atmosphere at the sea-level according to Bodhaine et al. (1999).

Wavelength (nm)	Rayleigh optical depth
470	0.1844
660	0.0461
865	0.0155